PHILOSOPHICAL TRANSACTIONS A

rsta.royalsocietypublishing.org

Research

Cite this article: Chaunsali R, Kim E, Yang J. 2018 Demonstration of accelerating and decelerating nonlinear impulse waves in functionally graded granular chains. *Phil. Trans. R. Soc. A* **376**: 20170136.
http://dx.doi.org/10.1098/rsta.2017.0136

Accepted: 5 March 2018

One contribution of 14 to a theme issue 'Nonlinear energy transfer in dynamical and acoustical systems'.

Subject Areas:
wave motion

Keywords:
tunable graded system, granular crystal, highly nonlinear waves

Author for correspondence:
Jinkyu Yang
e-mail: jkyang@aa.washington.edu

Demonstration of accelerating and decelerating nonlinear impulse waves in functionally graded granular chains

Rajesh Chaunsali[1], Eunho Kim[1,2,†] and Jinkyu Yang[1]

[1]Aeronautics and Astronautics, University of Washington, Seattle, WA 98195-2400, USA
[2]Division of Mechanical System Engineering & Automotive Hi-Technology Research Center, Chonbuk National University, 567 Baekje-daero, Deokjin-gu, Jeonju-si, Jeollabuk-do 54896, Republic of Korea

JY, 0000-0003-1547-0219

We propose a tunable cylinder-based granular system that is functionally graded in its stiffness distribution in space. With no initial compression given to the system, it supports highly nonlinear waves propagating under an impulse excitation. We investigate analytically, numerically and experimentally the ability to accelerate and decelerate the impulse wave without a significant scattering in the space domain. Moreover, the gradient in stiffness results in the scaling of contact forces along the chain. We envision that such tunable systems can be used for manipulating highly nonlinear impulse waves for novel sensing and impact mitigation purposes.

This article is part of the theme issue 'Nonlinear energy transfer in dynamical and acoustical systems'.

1. Introduction

A granular crystal is a closely packed assembly of systematically arranged granules that generally interact as per the Hertzian contact law. These discrete platforms have become increasingly popular in recent years due to their intrinsic tunability in terms of supporting a wide range of interesting wave physics spanning across linear, weakly nonlinear and strongly nonlinear regimes. Consequently, based on the rich wave physics,

†Equally contributed first author.

THE ROYAL SOCIETY PUBLISHING

researchers have proposed their use in a plethora of engineering applications, e.g. impact mitigation, signal filtering, energy harvesting and non-destructive evaluation [1–5].

The most fundamental granular crystal is a one-dimensional (1D) assembly of monodisperse spheres, i.e. a homogeneous spherical granular chain. If there is no initial compressive force applied to the chain, conventional linear elastic waves are forbidden to propagate due to the *essential* nonlinearity of the Hertzian contact law [6]. Nesterenko, in his pioneering work, showed that this 'sonic vacuum' rather supports a localized nonlinear travelling wave, i.e. solitary wave, under an impulse given to the chain [1]. The emergence of this wave solution is generally understood as an exquisite balance between nonlinearity and dispersion in the system. Since then, the propagation of strongly nonlinear impulse waves in many variants of this chain has been studied by several researchers (see some reviews, e.g. [2,7,8]).

Among such variants, we focus on a non-periodic granular system that is functionally graded in space. We note in passing that functionally graded architectures have been widely adopted in engineering, particularly for designing thermal barrier coatings. The feasibility of manufacturing such materials also motivated studies on wave propagation in functionally graded elastic solids [9,10]. While these previous studies employed *continuum* systems with gradient material properties, such as elastic modulus and density (volume fraction), we focus on *discrete* granular systems with a spatial gradient in mass or contact stiffness. Sen *et al.* first proposed such a system, which they called a 'tapered' chain [11]. This consists of a chain of spherical beads of decreasing radii. The mismatch of masses leads to the spreading of an impulse wave as it travels with the decreasing kinetic energy of the wave front. This eventually results in less contact force experienced in the latter part of the chain. This phenomenon was later verified by experiments as well [12–14]. In parallel, several studies have employed the collision models to gain theoretical understanding of energy propagation in such chains [15–19]. These previous studies have successfully demonstrated versatile wave dynamics in non-periodic, graded granular systems, such as impulse dispersion and shock mitigation, that are unprecedented in homogeneous granular chains. However, the physical systems that they employed have been limited primarily to sphere-based granular chains, which do not offer a rich design freedom to alter the system configurations *in situ*.

To tackle such a challenge, here we propose a functionally graded cylinder-based granular system, which provides extreme tunability by manipulating the stiffness gradient in 1D space. Note that the tapered granular chain proposed by Sen *et al.* results in a gradient of *both* mass and stiffness; however, a graded platform that can alter only one parameter freely—particularly stiffness—has not been thoroughly investigated. Therefore, a study of the wave propagation in such an 'intermediate' system, between Nesterenko's homogeneous granular chain and Sen's tapered granular chain, could shed new light on the strongly nonlinear wave phenomena in functionally graded systems. Furthermore, by leveraging the intrinsic tunability, this cylinder-based granular system might lead to interesting engineering applications for enhancing stress wave management.

The use of cylinders along with spherical granules was first proposed to enhance tunability in terms of independently changing particle masses [20]. However, later designs based solely on cylinders, interacting as per the Hertzian contact law, offered enhanced tunability. For example, contact stiffness can be tuned *in situ* simply by changing the contact angle between cylinders [21]. Moreover, for long cylinders, their bending can be invoked to include local resonance effects in wave propagation [22]. Therefore, such systems have recently become popular to demonstrate a wide span of wave phenomena. In linear regimes, these have been used for creating tunable bandgaps [22–24], topological defects [25], a mechanical non-reciprocal device [26,27] and Wannier–Stark ladders [28]. In addition, these systems have been used to manipulate strongly nonlinear impulse waves [21,29–31], along with possible extensions to three dimensions (3D) [32].

In this study, we create a table-top model of the functionally graded chain with an increasing and decreasing linear stiffness distribution in space by *in situ* tuning of contact angles between cylinders. We experimentally demonstrate that, without significant scattering of the wave front, the system can either accelerate or decelerate the impulse wave. We use numerical simulations to

corroborate our findings. Moreover, we employ the binary collision approximation (BCA) [16,18], which agrees well with numerical and experimental results in predicting the speed of the wave front. By investigating the spectral characteristics of the velocity profile of the travelling wave, we observe that these graded systems support a cascading of frequencies as the wave travels along the chain; however, the wave front remains nearly localized (maintaining the spatial width) in the space domain, as there is no obvious cascading of wavenumber. Moreover, the system offers the scaling of the maximum contact forces depending on the stiffness variation along the chain. The numerical results for this scaling agree well with the BCA predictions.

2. Experimental set-up

Our set-up consists of 40 identical short cylinders (radius $r = 9$ mm and height $h = 18$ mm) made of fused quartz (Young's modulus $Y = 72$ GPa, Poisson's ratio $\nu = 0.17$ and density $\rho = 2200\,\mathrm{kg\,m^{-3}}$) stacked on top of each other to form a chain, as shown in figure 1. We designed 3D-printed enclosures to support the cylinders, and those can be independently rotated to change their contact angles, as shown in the lower left inset of figure 1. We dropped a spherical quartz striker (radius $r = 9$ mm, mass $m_0 = 8.1$ g and velocity $v_0 = 0.8\,\mathrm{m\,s^{-1}}$) on the top of the chain to induce an impulse wave in the system. We then measure the velocity of each cylinder one by one using a laser Doppler vibrometer (LDV). Note that the enclosures have dedicated holes in them for the passage of the laser beam. The cylinders interact through the contacts, and the contact stiffness can be controlled by altering the contact angles. We maintain contact angles ranging from $\alpha = 2^\circ$ at one end to $\alpha = 90^\circ$ at the other, and enforce a *linear* gradient in the contact stiffness coefficient β (detailed in the following section). These angles are simply reversed to test two cases, i.e. a positive and a negative gradient in contact stiffness.

3. Modelling

We model the system with the discrete element method [33] as a 1D chain, in which each cylinder is approximated as a lumped mass ($m = \rho\pi r^2 h$) and is connected to neighbouring masses with a nonlinear spring element (upper left inset of figure 1). This spring follows the Hertzian contact law given by force $F = \beta(\alpha)[\delta x]_+^{n-1}$, where $\beta(\alpha)$ is the contact stiffness coefficient dependent on contact angle α, δx is the relative displacement, $n\,(=5/2)$ is the potential exponent, and the symbol $[\cdot]_+$ indicates that the contact force is 0 for non-positive values of δx. One can calculate β as [6]

$$\beta(\alpha) = \frac{2Y}{3(1-\nu^2)}\sqrt{\frac{r}{\sin\alpha}}\left[\frac{2K(e)}{\pi}\right]^{-3/2} \times \left\{\frac{4}{\pi e^2}\sqrt{\left[\left(\frac{a}{b}\right)^2 E(e) - K(e)\right][K(e) - E(e)]}\right\}^{1/2}. \tag{3.1}$$

Here, e is the eccentricity of the elliptical contact area between two cylinders and equals $\sqrt{1-(b/a)^2}$, with a and b being the semi-major and semi-minor axis length, respectively. Moreover, the ratio can be expressed as $b/a \approx [(1+\cos\alpha)/(1-\cos\alpha)]^{-2/3}$. $K(e)$ and $E(e)$ are the complete elliptical integrals of the first and second kinds, respectively. In this way we use the fact that a change in the contact angle leads to a change in the contact stiffness, and thus we can easily tune the stiffness gradient in the system.

For the first case of the functionally graded configurations considered in this study, we maintain a contact angle of 2° at the start of the chain (between the first and second cylinders from the top) and an angle of 90° at the end of the chain (between the 39th and 40th cylinders from the top). The rest of the contact angles are chosen such that the contact stiffness coefficient β from equation (3.1) varies linearly along the chain from $7.27 \times 10^{10}\,\mathrm{N\,m^{-1.5}}$ to $4.68 \times 10^{9}\,\mathrm{N\,m^{-1.5}}$. The higher the contact angle is, the lower the stiffness becomes. Therefore, this represents a case of a linear decrease in stiffness along the chain. For the second case, we simply reverse the contact angles along the chain, so that it represents a case of a linear increase in stiffness. We ignore any

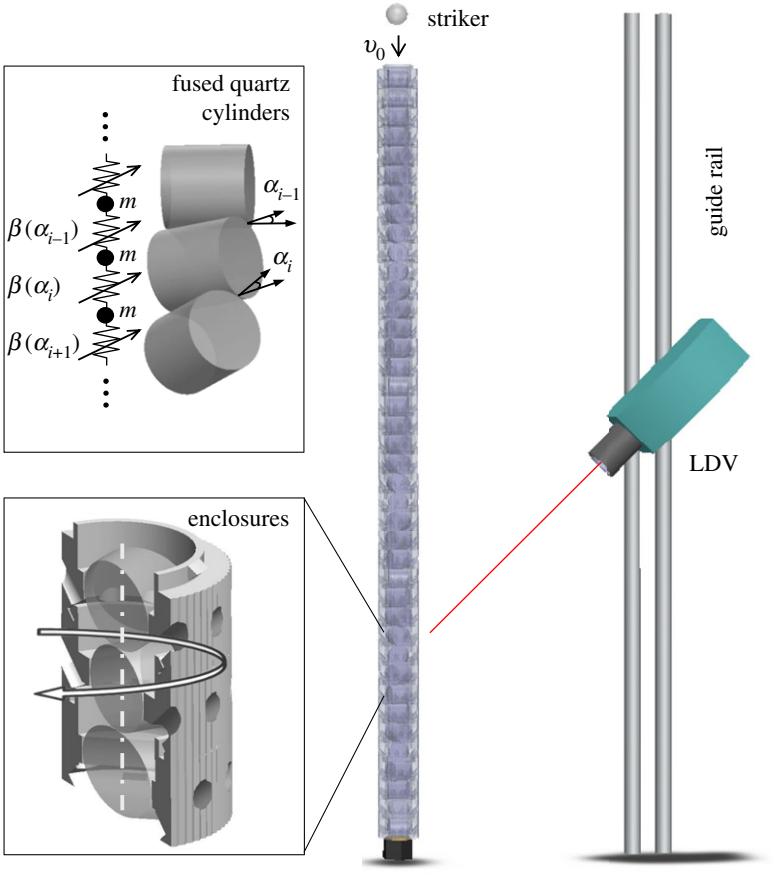

Figure 1. Experimental set-up: a vertical assembly of cylinders placed inside 3D-printed enclosures for support. Contact angles can be tuned *in situ*. After striking the chain, point-by-point measurement is performed by an LDV. (Online version in colour.)

material dissipation in the system. We also neglect the effect of gravity in this short chain, as the maximum compressive load due to gravity is about 1.6 N at the bottom of the chain, which is about two orders of magnitude less than the contact forces induced by the impulse, as shown in the later sections.

To solve this nonlinear system numerically, we write the following equation of motion for the cylinders (with position index $i = 1, 2, 3, \ldots$)

$$m\frac{\mathrm{d}^2 x_i}{\mathrm{d}t^2} = \beta_{i-1}[x_{i-1} - x_i]_+^{n-1} - \beta_i[x_i - x_{i+1}]_+^{n-1}, \tag{3.2}$$

where x_i denotes the dynamic displacement, β_i is a simplified notation for $\beta(\alpha_i)$ used hereafter, and indexing i starts from the top of the vertical chain. Note that $\beta_0 = 3.98 \times 10^9\,\mathrm{N\,m^{-1.5}}$, which is calculated by considering a sphere-to-cylinder contact between the striker and the first cylinder. We solve this system of equations using the ODE45 solver in MATLAB with the initial condition given in the form of striker velocity $v_0 = 0.8\,\mathrm{m\,s^{-1}}$.

To get further insights into the wave dynamics of this graded system, we employ the BCA [16]. This method considers the interaction of only two masses at a time. First, by applying the conservation of energy in our dissipation-less model, we calculate the time it takes for the ith mass to completely transfer its momentum to the $(i+1)$th mass. We use the exact solution for this

'residence time' derived in ref. [18] to write

$$T_i = \sqrt{\pi}\left(\frac{n\mu_i}{2\beta_i}\right)^{1/n} v_i^{-1+2/n}\frac{\Gamma(1+1/n)}{\Gamma(1/2+1/n)}, \tag{3.3}$$

where $\mu_i = m_i m_{i+1}/(m_i + m_{i+1})$ denotes the reduced mass of interacting masses m_i and m_{i+1}, and v_i is the maximum velocity of the ith mass. This velocity of the ith cylinder can be calculated from the velocity of its previous $(i-1)$th cylinder simply by applying the conservation of linear momentum. Therefore

$$v_i = \frac{2v_{i-1}}{1 + m_i/m_{i-1}}. \tag{3.4}$$

We know that all the cylinders are identical in mass ($m_i = m\ \forall\, i \geq 1$), thus the velocity of all the cylinders would be the same. However, due to the mass mismatch between the first cylinder ($i = 1$) and the striker ($i = 0$), we would have the following relation:

$$v_i = v_1 = \frac{2v_0}{1 + m/m_0} \quad \forall\, i \geq 2. \tag{3.5}$$

Once we have the velocity of each mass, we can calculate the residence time for each cylinder from equation (3.3). This can be used to calculate the wave speed V at the ith cylinder as

$$V_i = \frac{2r}{T_i}. \tag{3.6}$$

Moreover, the total time taken by the wave to pass the ith cylinder can be calculated as

$$t_i = \sum_{j=1}^{i} T_j. \tag{3.7}$$

4. Results and discussion

(a) Accelerating and decelerating nonlinear waves

We show the spatio-temporal evolution of the cylinders' velocities in figure 2. Numerical and analytical results for the chain with decreasing stiffness along its length are shown in figure 2*a*. We notice that, as the wave front evolves over time, it slows down by curving upwards in the spatio-temporal map. Moreover, the wave front does not show significant scattering. As a result, the velocity amplitude of the cylinders does not show a large variation along the chain, complying well with the assumption in the BCA that binary collisions between cylinders transfer the same velocity along the chain (equation (3.5)). Therefore, the analytical solution obtained from equation (3.7) shows a good agreement with the numerically obtained wave front. We also notice that this wave front is followed by other pulses whose characteristics are similar to the former. These waves emerge because of the large stiffness mismatch between the first contact (between the striker and first cylinder) and the second contact (between the first and second cylinders) in the chain. In figure 2*b*, we show the experimentally obtained velocity map for this graded chain. A good match with the numerical results is evident. This, therefore, demonstrates the impulse deceleration capability of our system.

Figure 2*c* shows numerical and analytical predictions for the reverse chain with increasing contact stiffness. We clearly see the acceleration of the wave front in this case, with a good agreement with the BCA predictions. Note that this case does not cause multiple wave fronts, as shown in figure 2*a*. This is because of the small stiffness mismatch between the first two contacts in the chain. We see that these numerical predictions are in agreement with experimental results, as shown in figure 2*d*. This demonstrates impulse acceleration in our tunable system. Minor scattering shown in experimental data (figure 2*b*,*d*) is due to variations in the setting of contact angles in the experiment set-up.

In order to get further insights into the system, we extract more information, such as residence time and wave speed, from the velocity maps shown in figure 2. We calculate residence time

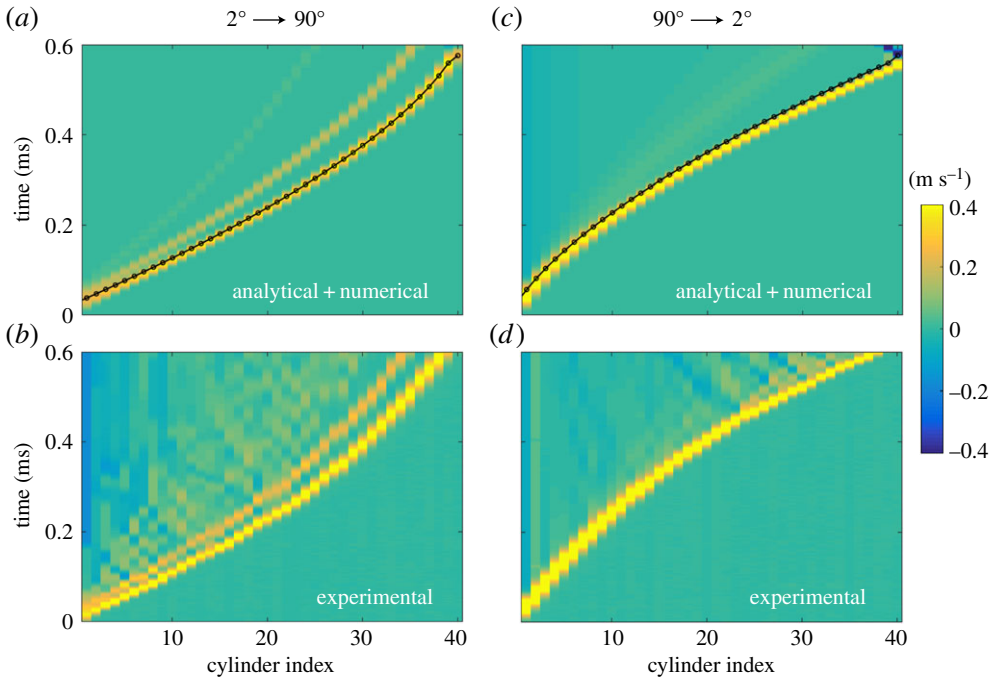

Figure 2. Spatio-temporal velocity map. (*a*) Numerical velocity map of the graded chain with angles varying from 2° to 90° along the chain. Wave trajectory obtained through analytical method (black line) is superimposed on the map, closely following the wave front. (*b*) Experimentally obtained velocity map for the same case. (*c*) Numerical and analytical results for the graded chain with angles varying from 90° to 2° along the chain. (*d*) Experimental velocity map for the same case. (Online version in colour.)

analytically using equation (3.3) for every cylinder location. For comparison, we extract the same for the wave front in numerical and experimental maps in the following way. Given the velocity profiles, we define the residence time for the ith cylinder as the interval between t_i^{i} and t_i^{f}. Here, t_i^{i} is the time at which the velocity of the ith cylinder exceeds the velocity of the $(i-1)$th cylinder, and t_i^{f} is the time at which the velocity of the $(i+1)$th cylinder exceeds the velocity of the ith cylinder. We plot the results in figure 3*a*,*b* for the chains with decreasing and increasing stiffness, respectively. The decrease in the stiffness along the chain (figure 3*a*) is clearly reflected in the increase of the residence time. Similarly, the increase in the stiffness along the chain (figure 3*b*) is reflected in the decrease of the residence time. We observe that the experimental data follow the trend predicted by the analytical and numerical methods.

We calculate wave speed from residence time by using equation (3.6) and show this in figure 3*c*,*d* for the respective chains. We observe that the experimental data have a large variation in its values along the length of the chains. So we use a power-law fit to better interpret the experimental wave speed. This makes sense because we can deduce $V_i \propto \beta_i^{1/n}$ from equation (3.3) and equation (3.6). The linearly varying β_i in our system can be expressed as $\beta_i = b_1 + b_2 i$. Therefore, we use the relation $V_i = (b_1 + b_2 i)^{1/n}$ to obtain a fit for experimental wave speeds. We note that this wave speed closely follows the trends predicted by the analytical and numerical methods. However, we observe that it is relatively small in value. This may be because of several factors, including (1) the presence of dissipation in experiments, which is not accounted for in the numerical and analytical calculations, and (2) variation in the power law (value of n) for cylindrical contact as one goes from small angles to high angles [21].

One may now ask the following question: How can this acceleration and deceleration of the impulse wave be enhanced further in the context of any practical applications? One of the solutions is to introduce an inertial mismatch along the chain. The cylinder-based system provides

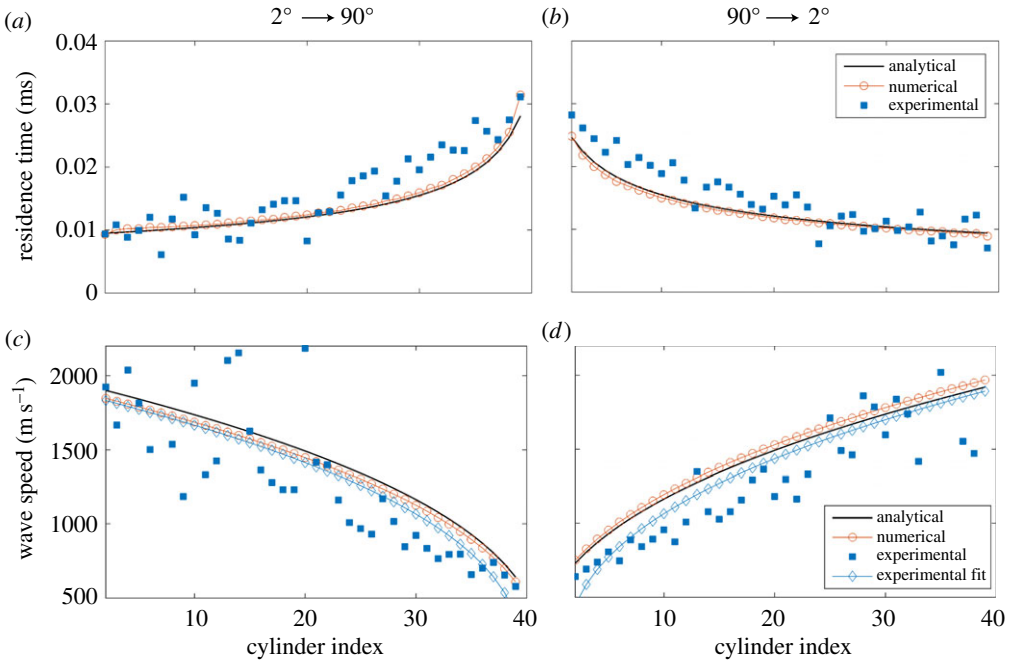

Figure 3. (*a*) Residence time for the wave front calculated along the chain (2° to 90°). Increasing residence time indicates stiffness decrease along the chain. (*b*) The same calculated for the reverse chain. (*c*,*d*) Wave speeds obtained from the corresponding residence times. A power-law fit is used to obtain smooth experimental data. (Online version in colour.)

a unique advantage in this regard. The heights of the cylinders can be varied *independently*, so that we introduce a mass gradient without changing the stiffness gradient. Therefore, by following the conservation of linear momentum, it is straightforward to conclude that the wave deceleration caused by a *decreasing stiffness* in figure 3*c* can be enhanced by setting an *increasing mass* gradient. Similarly, the wave acceleration caused by an *increasing stiffness* in figure 3*d* can be enhanced by setting a *decreasing mass* gradient (see appendix A for some exemplary cases analysed numerically).

(b) Spectrum

In this section, we discuss the spectral characteristics of the nonlinear impulse propagating in the graded chain. We use only numerical simulations hereafter. For better data visualization, we consider a longer chain with 200 cylinders. Moreover, to get rid of multiple waves emerging from the striker impact as shown in figure 2*a*, we use a striker with the same mass as that of cylinders, and equate its contact stiffness (β_0) to β_1. Figure 4 shows the velocity maps for these long chains and frequency/wavenumber extracted from the same by employing the fast Fourier transformation. For the case of decreasing stiffness (figure 4*a*), we see that the impulse slows down as it propagates along the chain. We plot its frequency spectrum in figure 4*b*. It shows a clear cascading of frequencies, i.e. spectral energy shifts to lower frequencies along the chain. This is a reflection of higher residence time observed in figure 3*a* due to the decrease in stiffness. However, the wavenumber calculated at each time instant in figure 4*c* shows an interesting trend. There is no such clear cascading. As we have already discussed that the height of the wave front (i.e. velocity amplitude) remains nearly intact (equation (3.5)), the absence of cascading in wavenumber means that the wave front is nearly localized in space and maintains its spatial width without significant scattering (see the velocity–time history of the 100th cylinder in the inset of figure 4*a*). Similarly, the results for the reverse chain can be interpreted as in figure 4*d*–*f*. Unlike

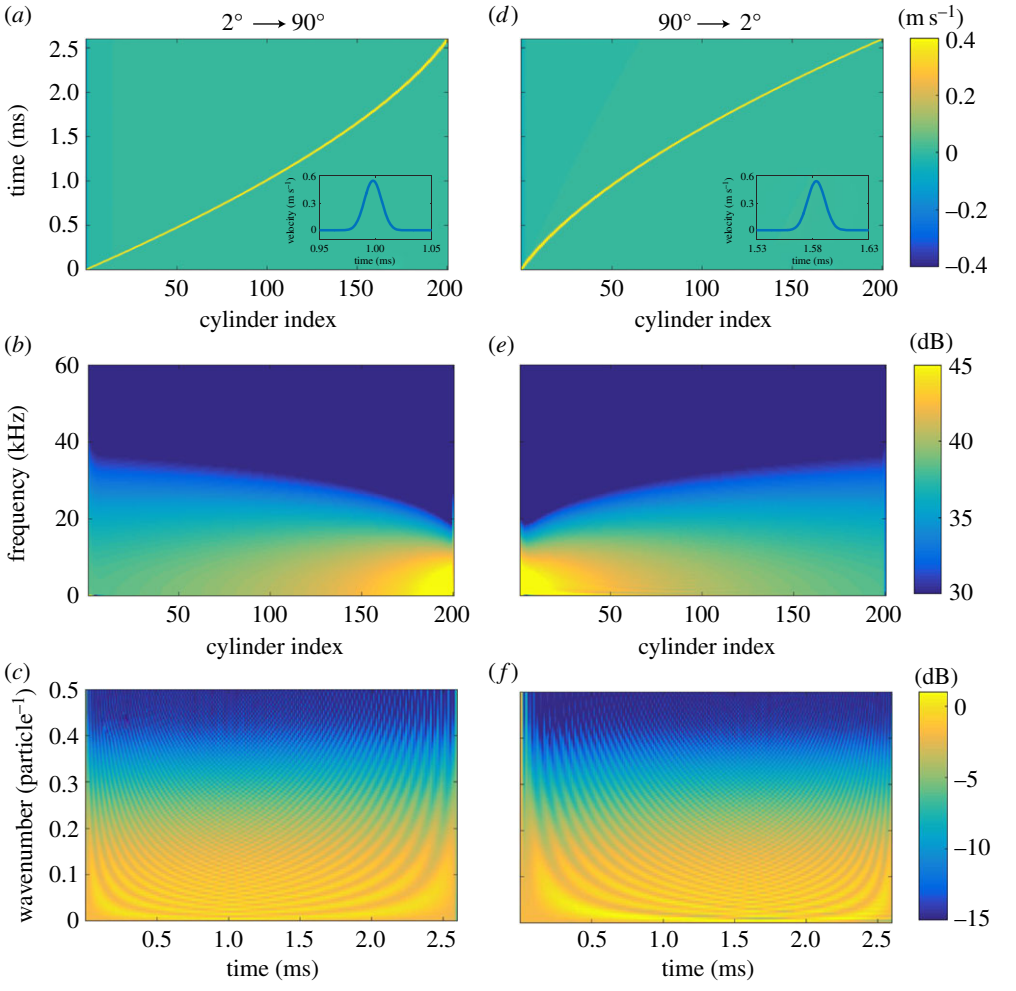

Figure 4. Spectral characteristics of graded chain. (*a*) Numerically obtained spatio-temporal velocity map for a longer graded (2° to 90°) chain. Inset shows velocity–time profile of 100th cylinder. (*b*) Its spectrum calculated in the time domain, i.e. frequency, along the chain length. (*c*) Its spectrum calculated in the space domain, i.e. wavenumber, against time. (*d–f*) The same for the reverse chain. (Online version in colour.)

the case of decreasing stiffness, we observe the spreading of the energy to a broader spectrum of frequency in this increasing stiffness case (compare figure 4*b*,*e*). However, in the wavenumber domain, the localization trends are similar between the two cases. Previous studies on tapered granular chains [11] showed acceleration and deceleration of the wave front; however, the width and the kinetic energy of the wave front change due to scaling in both mass and stiffness along the chain. Unlike the tapered chain, our current system offers the tunability of impulse speed with contact force scaling (discussed next) but preserving the spatial width and the kinetic energy of the wave front.

(c) Contact force scaling

We extract the maximum contact force values (CF_{max}) at each cylinder location for the system discussed in figure 4 and plot them in figure 5. We clearly notice that this graded chain provides varying contact force along the chain depending on the stiffness gradient in figure 5*a*,*b*. Also note in the inset a typical force–time history profile at the middle of the chain. To evaluate the dependence of this contact force on stiffness coefficient, we plot them in a logarithmic

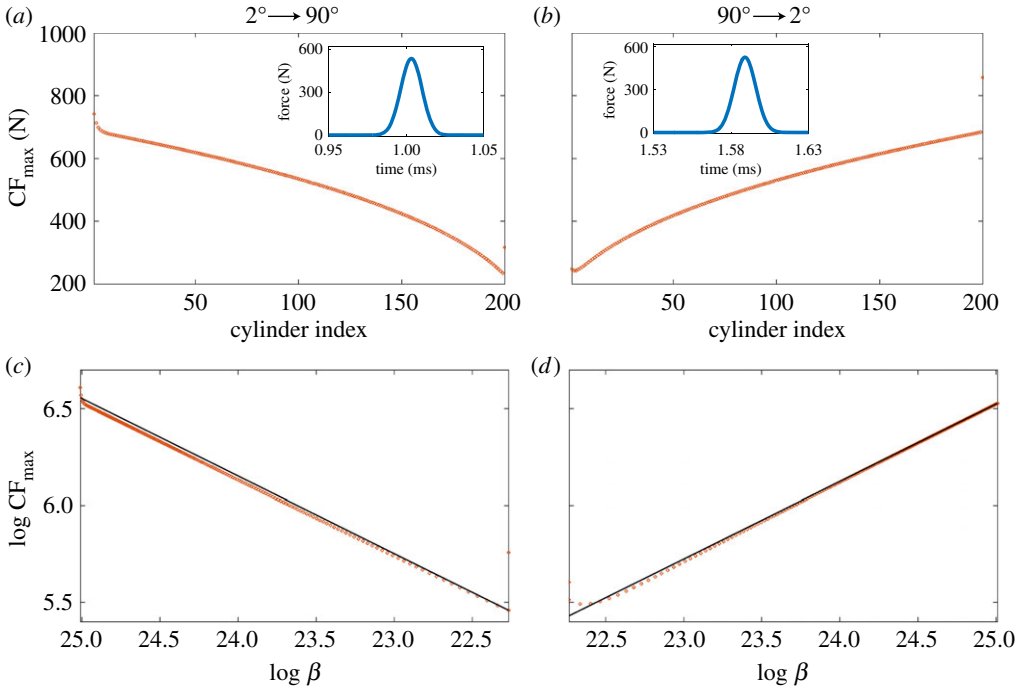

Figure 5. Scaling of contact force. (*a*) Numerically obtained maximum contact force variation along the chain for the same system as shown in figure 4. Inset shows force–time profile at the contact between 99th and 100th cylinders. (*b*) The same for the reverse chain. (*c*,*d*) Maximum contact force versus contact stiffness (circles) for the respective chains shows a power law. A black line with slope equal to that power guides the eyes. Note the reverse values on the *x*-axis for (*c*). (Online version in colour.)

scale in figure 5*c*,*d*, which show a linear trend. This power-law scaling can be understood from the BCA predictions. One can calculate the maximum compression at the *i*th contact as $\delta x_{\max,i} = (n\mu_i v_i/2\beta_i)^{1/n}$ [18]. This means that the maximum contact force $\mathrm{CF}_{\max,i} = \beta_i \delta x_{\max,i}^{n-1}$ from the contact law, and therefore, $\mathrm{CF}_{\max,i} \propto {\beta_i}^{1/n}$. In figure 5*c*,*d*, we plot a black line with the slope equal to $1/n = 2/5$, to show the remarkable agreement of numerical simulations to the scaling law predicted by the BCA.

5. Conclusion

We have demonstrated the impulse acceleration and deceleration capability of cylinder-based functionally graded granular chains. The architecture allows us to have *in situ* control over stiffness distribution, and therefore it offers extreme tunability. We showed that space–time evolution of the wave front in the experiments is well predicted by numerical and analytical calculations. The spectral characteristics obtained from the velocity profile of the wave propagating in such systems show a clear cascading of frequencies, but not of wavenumbers. This means that, even though the impulse accelerates/decelerates along the chain, it does not show significant scattering and remains localized in the space domain by retaining its spatial width. Finally, we verified that the contact forces along the chain follow a power-law scaling depending on the stiffness distribution, and this complies well with the analytical predictions. The proposed system can be potentially used for manipulating stress waves under an impact in various engineering applications. Further studies include the effect of plasticity and viscoelasticity in such a system, and also its generalizations to build tunable architectures in higher dimensions.

Data accessibility. The data set analysed during the current study is available from the corresponding author on reasonable request.

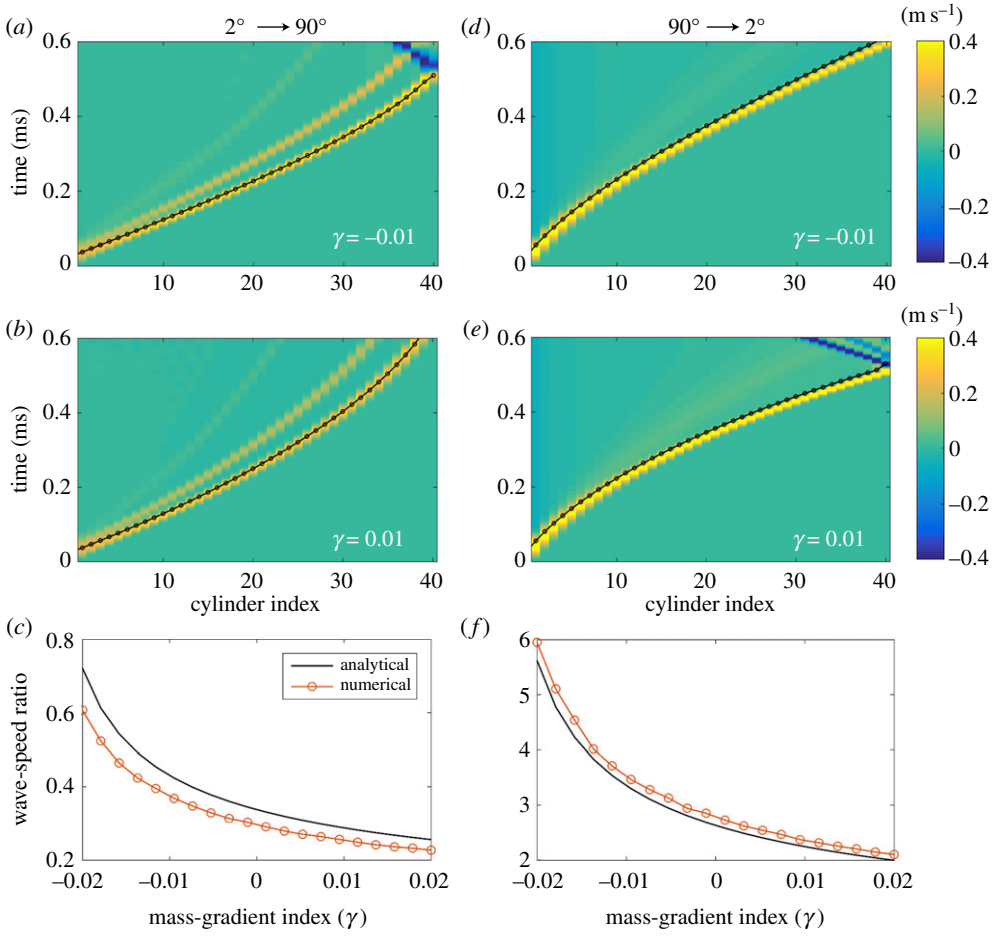

Figure 6. Effect of mass gradient. (*a*) Numerical velocity map of the graded chain with angles varying from 2° to 90° and with a decreasing mass gradient ($\gamma = -0.01$). Spatio-temporal evolution of the wave front is also well captured by the analytical method (black line). (*b*) Keeping the same stiffness gradient but reversing the mass gradient ($\gamma = 0.01$). (*c*) Wave-speed ratio (V_{out}/V_{in}) calculated at multiple mass-gradient values indicating the effect on impulse wave deceleration. (*d–f*) The same but with reverse stiffness gradient, and the effect on impulse wave acceleration. (Online version in colour.)

Authors' contributions. E.K. and J.Y. conceived and designed the study. E.K. performed the experiments. R.C. and E.K. performed numerical and analytical calculations, performed data analysis and interpreted the results. R.C. drafted the manuscript, and all the authors were involved in finalizing the manuscript.

Competing interests. The authors declare that they have no competing interests.

Funding. J.Y. gratefully appreciates the support from the NSF (CAREER-1553202) and AFOSR (FA9550-17-1-0114). E.K. acknowledges the support from the National Research Foundation of Korea (NRF) grant funded by the Korean government (NRF-2017R1C1B5018136).

Acknowledgements. We thank the editors of this special issue for their invitation. We acknowledge the assistance by Sean E. Phenisee and Matthew Toles in the design of the 3D-printed enclosure structure.

Appendix A. Effect of inertial mismatch in accelerating and decelerating impulse waves

In this section, we numerically study the effect of introducing inertial mismatch (i.e. gradient in mass) in our system in addition to a stiffness gradient. To that end, we keep all the conditions the same as those in figures 2 and 3, but introduce a linear gradient in mass such that $m_i =$

$m(1+\gamma i)$ $\forall i \in [1, 40]$. Note that both positive and negative gradient (γ) can be introduced, irrespective of the stiffness gradient, by changing the heights of the cylinders.

Figure 6 shows some exemplary cases, in which the introduction of mass gradient in the system affects the impulse deceleration and acceleration phenomena. In figure 6*a*, decreasing mass along the chain forces the wave front to travel faster, and therefore the wave deceleration caused by decreasing stiffness is weakened (compare figure 6*a* and figure 2*a*). However, increasing mass in figure 6*b* complements the wave deceleration capability of the system with decreasing stiffness (compare figure 6*b* and figure 2*a*). We calculate the wave speed numerically and analytically as shown in figure 3*c*, and further extract the quantity $V_{\text{out}}/V_{\text{in}}$, i.e. the ratio of wave speeds at the output and the input of the system. In figure 6*c*, we plot this wave-speed ratio as a function of mass-gradient index (γ). It is clear that a ratio less than 1 indicates the wave deceleration along the chain; however, it is dependent on mass-gradient index. Therefore, positive mass gradient can further enhance wave deceleration for this stiffness configuration of the system. The same procedure is followed for the configuration with the increasing stiffness along the chain and plotted in figure 6*d–f*. We observe from figure 6*f* that the impulse wave can be further accelerated with negative mass gradient. It would be an interesting exercise for the future to see to what extent the mass gradient can be introduced in real experimental set-ups. This is because increasing heights of the cylinders would also introduce local resonance effects [22,29], and that can potentially have qualitative effects on the impulse wave propagation.

References

1. Nesterenko V 2001 *Dynamics of heterogeneous materials*. Berlin, Germany: Springer.
2. Sen S, Hong J, Bang J, Avalos E, Doney R. 2008 Solitary waves in the granular chain. *Phys. Rep.* **462**, 21–66. (doi:10.1016/j.physrep.2007.10.007)
3. Porter MA, Kevrekidis PG, Daraio C. 2015 Granular crystals: nonlinear dynamics meets materials engineering. *Phys. Today* **68**, 44–50. (doi:10.1063/PT.3.2981)
4. Yang J, Silvestro C, Sangiorgio SN, Borkowski SL, Ebramzadeh E, De Nardo L, Daraio C. 2012 Nondestructive evaluation of orthopaedic implant stability in THA using highly nonlinear solitary waves. *Smart Mater. Struct.* **21**, 012002. (doi:10.1088/0964-1726/21/1/012002)
5. Ni X, Rizzo P, Yang J, Khatri D, Daraio C. 2012 Monitoring the hydration of gypsum cement with highly nonlinear solitary waves. *NDT & E* **52**, 76–85. (doi:10.1016/j.ndteint.2012.05.003)
6. Johnson K. 1985 Normal contact of elastic solids—Hertz theory. In *Contact mechanics*, pp. 84–106. Cambridge, UK: Cambridge University Press. (doi:10.1017/CBO9781139171731.005).
7. Chong C, Porter MA, Kevrekidis PG, Daraio C. 2017 Nonlinear coherent structures in granular crystals. *J. Phys. Condens. Matter* **29**, 413003. (doi:10.1088/1361-648X/aa7672)
8. Starosvetsky Y, Jayaprakash KR, Vakakis AF. 2017 Traveling and solitary waves in monodisperse and dimer granular chains. *Int. J. Mod. Phys. B* **31**, 1742001. (doi:10.1142/S0217979217420012)
9. Chiu T-C, Erdogan F. 1999 One-dimensional wave propagation in a functionally graded elastic medium. *J. Sound Vib.* **222**, 453–487. (doi:10.1006/jsvi.1998.2065)
10. Bruck HA. 2000 A one-dimensional model for designing functionally graded materials to manage stress waves. *Int. J. Solids Struct.* **37**, 6383–6395. (doi:10.1016/S0020-7683(99)00236-X)
11. Sen S, Manciu FS, Manciu M. 2001 Thermalizing an impulse. *Physica A* **299**, 551–558. (doi:10.1016/S0378-4371(01)00340-5)
12. Nakagawa M, Agui JH, Wu DT, Extramiana DV. 2003 Impulse dispersion in a tapered granular chain. *Granul. Matter* **4**, 167–174. (doi:10.1007/s10035-002-0119-1)
13. Melo F, Job S, Santibanez F, Tapia F. 2006 Experimental evidence of shock mitigation in a Hertzian tapered chain. *Phys. Rev. E* **73**, 41305. (doi:10.1103/PhysRevE.73.041305)
14. Doney RL, Agui JH, Sen S. 2009 Energy partitioning and impulse dispersion in the decorated, tapered, strongly nonlinear granular alignment: a system with many potential applications. *J. Appl. Phys.* **106**, 64905. (doi:10.1063/1.3190485)
15. Wu DT. 2002 Conservation principles in solitary impulse propagation through granular chains. *Physica A* **315**, 194–202. (doi:10.1016/S0378-4371(02)01240-2)

16. Rosas A, Lindenberg K. 2004 Pulse velocity in a granular chain. *Phys. Rev. E* **69**, 37601. (doi:10.1103/PhysRevE.69.037601)
17. Doney RL, Sen S. 2005 Impulse absorption by tapered horizontal alignments of elastic spheres. *Phys. Rev. E* **72**, 41304. (doi:10.1103/PhysRevE.72.041304)
18. Harbola U, Rosas A, Esposito M, Lindenberg K. 2009 Pulse propagation in tapered granular chains: an analytic study. *Phys. Rev. E* **80**, 31303. (doi:10.1103/PhysRevE.80.031303)
19. Machado LP, Rosas A, Lindenberg K. 2013 Momentum and energy propagation in tapered granular chains. *Granul. Matter* **15**, 735–746. (doi:10.1007/s10035-013-0444-6)
20. Herbold EB, Kim J, Nesterenko VF, Wang SY, Daraio C. 2009 Pulse propagation in a linear and nonlinear diatomic periodic chain: effects of acoustic frequency band-gap. *Acta Mech.* **205**, 85–103. (doi:10.1007/s00707-009-0163-6)
21. Khatri D, Ngo D, Daraio C. 2012 Highly nonlinear solitary waves in chains of cylindrical particles. *Granul. Matter* **14**, 63–69. (doi:10.1007/s10035-011-0297-9)
22. Kim E, Yang J. 2014 Wave propagation in single column woodpile phononic crystals: formation of tunable band gaps. *J. Mech. Phys. Solids* **71**, 33–45. (doi:10.1016/j.jmps.2014.06.012)
23. Li F, Ngo D, Yang J, Daraio C. 2012 Tunable phononic crystals based on cylindrical Hertzian contact. *Appl. Phys. Lett.* **101**, 171903. (doi:10.1063/1.4762832)
24. Meidani M, Kim E, Li F, Yang J, Ngo D. 2015 Tunable evolutions of wave modes and bandgaps in quasi-1D cylindrical phononic crystals. *J. Sound Vib.* **334**, 270–281. (doi:10.1016/j.jsv.2014.09.010)
25. Chaunsali R, Kim E, Thakkar A, Kevrekidis PG, Yang J. 2017 Demonstrating an in situ topological band transition in cylindrical granular chains. *Phys. Rev. Lett.* **119**, 24301. (doi:10.1103/PhysRevLett.119.024301)
26. Li F, Chong C, Yang J, Kevrekidis PG, Daraio C. 2014 Wave transmission in time- and space-variant helicoidal phononic crystals. *Phys. Rev. E* **90**, 53201. (doi:10.1103/PhysRevE.90.053201)
27. Chaunsali R, Li F, Yang J. 2016 Stress wave isolation by purely mechanical topological phononic crystals. *Sci. Rep.* **6**, 30662. (doi:10.1038/srep30662)
28. Shi X, Chaunsali R, Wu Y, Yang J. 2018 Elastic Wannier–Stark ladders and Bloch oscillations in 1D granular crystals. *J. Appl. Phys.* **123**, 104904. (doi:10.1063/1.5011664)
29. Kim E, Li F, Chong C, Theocharis G, Yang J, Kevrekidis PG. 2015 Highly nonlinear wave propagation in elastic woodpile periodic structures. *Phys. Rev. Lett.* **114**, 118002. (doi:10.1103/PhysRevLett.114.118002)
30. Kore R, Waychal A, Agarwal S, Yadav P, Uddin A, Sahoo N, Shelke A. 2016 Impact induced solitary wave propagation through a woodpile structure. *Smart Mater. Struct.* **25**, 25027. (doi:10.1088/0964-1726/25/2/025027)
31. Chaunsali R, Toles M, Yang J, Kim E. 2017 Extreme control of impulse transmission by cylinder-based nonlinear phononic crystals. *J. Mech. Phys. Solids* **107**, 21–32. (doi:10.1016/j.jmps.2017.06.015)
32. Kim E, Kim YHN, Yang J. 2015 Nonlinear stress wave propagation in 3D woodpile elastic metamaterials. *Int. J. Solids Struct.* **58**, 128–135. (doi:10.1016/j.ijsolstr.2014.12.024)
33. Cundall PA, Strack O. 1979 A discrete numerical model for granular assemblies. *Géotechnique* **29**, 47–65. (doi:10.1680/geot.1979.29.1.47)